Optical Materials 148 (2024) 114787

Contents lists available at ScienceDirect

Optical Materials

journal homepage: www.elsevier.com/locate/optmat

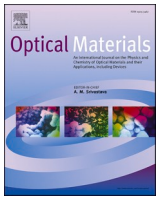

Research Article

Optoelectric response of Schottky photodiode with a PVP: $ZnTiO_3$ nanocomposite as an interfacial layer

Ali Barkhordari [a,*], Hamid Reza Mashayekhi [a], Pari Amiri [b], Şemsettin Altındal [c], Yashar Azizian-Kalandaragh [b,d,e,f]

[a] Faculty of Physics, Shahid Bahonar University of Kerman, Kerman, Iran
[b] Department of Engineering Sciences, Faculty of Advanced Technologies, Sabalan University of Advanced Technologies (SUAT), Namin, Iran
[c] Department of Physics, Faculty of Sciences, Gazi University, Ankara, Turkey
[d] Department of Photonics, Faculty of Applied Sciences, Gazi University, 06500, Ankara, Turkey
[e] Photonics Application and Research Center, Gazi University, 06500, Ankara, Turkey
[f] Department of Physics, University of Mohaghegh Ardabili, P.O. Box.179, Ardabil, Iran

ARTICLE INFO

Keywords:
Schottky photodiode (PD)
Nanocomposite
Zinc titanate ($ZnTiO_3$)
Photo-response
Electric properties

ABSTRACT

This work aims to study the photo-response of the fabricated silicon-based Al/PVP:$ZnTiO_3$/p-Si photodiode (PD) in a wide range of illumination intensities. To make a metal-polymer/nanocomposite-semiconductor (MPS) PD, a thin film of PVP:$ZnTiO_3$ nanocomposite is deposited at the interface of the metal-semiconductor (MS) structure. Information regarding the preparation and manufacturing procedures is provided. Through the examination of the current-voltage (I–V) behavior, essential electrical properties such as leakage current (I_0), barrier height (Φ_{B0}), ideality factor (n), series and shunt resistances (R_s, R_{sh}), energy-dependent interface states density (N_{ss}), photocurrent (I_{ph}), and photosensitivity (S) are acquired. The thermionic emission (TE) theory, along with the Norde and Cheung methods, is employed to calculate the parameters Φ_{B0}, n, and Rs. The values of Φ_{B0} and R_s are decreased by raising the illumination intensity while the n value is increased. In addition, the illumination coefficient (α) and the value of Φ_{B0} in the ideal case are determined from the Φ_{B0}-P and Φ_{B0}-n plots. The efficiency (η) of the sample is calculated at each illumination intensity whose maximum value is 2.30 % at the intensity of 450 mW/cm^2. The illumination-dependent photocurrent is investigated at the negative bias region that shows a good linear behavior in the ln(I_{ph})-ln(P) profile. The photosensitivity (S) of the fabricated PD is obtained as ~500 which is, compared with previous PDs. These findings demonstrate that the developed silicon-based MPS-type PD with a structure of Al/PVP:$ZnTiO_3$/p-Si exhibits a good photo-response and can successfully replace traditional MS PDs in optoelectronic and photovoltaic applications.

1. Introduction

Recently, the influence of using an organic or polymer interfacial layer instead of insulator or oxide interlayers on the illumination-dependent optical and electrical characteristics of Schottky photodiode (PD) devices has been thoroughly investigated since they allow modification of electrical parameters such as saturation current (I_0), photosensitivity (S), ideality factor (n), barrier height (BH), shunt/series resistances (R_{sh}, R_s), interface/surface states (N_{ss}), rectification rate (RR), open-circuit voltage (V_{oc}) [1–3]. All these variables are often influenced by the sample temperature, created interlayer at M/S interface, acceptor, or donor density (N_a or N_d), and the uniformity of the BH [4–6]. It is worth noting that interface states at the interlayer/semiconductor interface serve as recombination sites that seize and discharge an electric charge in response to changes in temperature and light. In other words, electric charges operate as charge carriers throughout the contact because they first trap in the restricted bandgap before migrating away from them [7]. These conditions can arise due to imperfections on the surface of the semiconductor, such as unpaired connections, deficiencies in oxygen atoms, the introduction of donor or acceptor atoms, irregularities within the semiconductor's structure, and the presence of various organic contaminants resulting from laboratory cleaning and preparation protocols [8]. Thus, scientists directed their efforts towards amplifying the electrical and optical characteristics

* Corresponding author.
E-mail address: alibarkhordari20@phy.uk.ac.ir (A. Barkhordari).

https://doi.org/10.1016/j.optmat.2023.114787
Received 17 October 2023; Received in revised form 6 December 2023; Accepted 22 December 2023
Available online 1 January 2024

through the utilization of an organic/polymer intermediate layer infused with a fitting metal or metal oxide. This approach sought to diminish the N_{ss} level, leakage current, Rs, while simultaneously enhancing BH, RR, and R_{sh}. Since polymers have been compared to insulators like SnO_2 and SiO_2, they stand out for having qualities like a high capacity for charge storage, an appropriate surface area to volume ratio, lightweight, excellent mechanical and dielectric strength, and straightforward growth techniques [9]. Despite this, polymers sadly have some flaws, like low mobility and dielectric permittivity. Nevertheless, by including different metals and metal oxides [10].

Both single materials and ZnO–TiO_2 composites attract significant attention because of the important effects and various applications offered by these two wideband semiconductors, namely TiO_2 and ZnO [11–13]. ZnO has garnered attention in the literature for its distinct characteristics and varied uses in see-through electronics, sensing devices for chemicals, devices utilizing piezoelectricity, spintronics, and emitters of ultraviolet (UV) light [14–17]. Compared to commonly used semiconductors like ZnSe and GaN for blue-green light-emitting devices, ZnO possesses a significant exciton binding energy of 60 meV, setting it apart [18].

However, TiO_2 is a semiconductor that is non-toxic, stable in aqueous solutions, and reasonably priced. Additionally, TiO_2's large band gap and the prolonged lifetime of photo-generated holes and electrons have contributed to the material's excellent photocatalytic properties [19]. TiO_2 does not use as much of the solar spectrum as other photocatalytic materials, and it has a relatively high rate of electron-hole recombination [20]. These problems can be resolved and the activity of TiO_2 photo-catalysts improved by ZnO doping [21]. There are several applications of the perovskite-type oxide structure of $ZnTiO_3$ such as microwave resonators [22], gas sensors [23] (for ethanol, NO, CO, and other gases), metal-air barriers [24], high-performance catalysts [25] for the total oxidation of hydrocarbons or CO and NO reduction [26], and paint pigment [27]. Numerous substances, such as Zn_2TiO_4 (cubic), Zinc Titanate ($ZnTiO_3$, cubic, and hexagonal), and $Zn_2Ti_3O_8$ (cubic), are found in the ZnO–TiO_2 system [28,29].

It is observed that the negative impacts of the interlayer, R_s, and N_{ss} cause the voltage-dependent current or capacitance/conductance to diverge from their ideal situations generally. For instance, the C–V profile occasionally exhibits an explicit peak due to R_s and N_{ss} in both the depletion and accumulation regions in several applications. The lnI-V graphs reveal similar results. It is very evident that there is the interface deflect and N_{ss}, resulting in the deviation of these graphs from linearity, especially at larger forward bias voltage [30].

In semiconductor devices, the resistance (R_s) usually stems from various factors, including the back ohmic contact and the front Schottky contacts, interfacial layer and bulk resistance of semiconductor, as well as the used metal wires to perform electric measurements. Additionally, the presence of dislocations, and surface impurities resulting in the non-uniform or heavily doped regions in the semiconductor contribute to R_s [4,30]. On the other hand, the shunt resistance (R_{sh}) is typically caused by physical flaws within the interlayer, such as holes or gaps, and areas of high conductivity like grain boundaries or dislocations [5,6]. Depending on the applied voltage, a similar orientation occurs in both external and internal electric fields at reverse bias voltages [31]. Therefore, the entire electric field in this situation is more powerful than it was in the forward bias voltage. Several e-h pairs form at the contact point of a photodiode subjected to illuminations ($=hc/q > E_g$), and electrons might be recombined. However, because the illumination effect reduces the recombination of the electron-hole pairs, photocurrent rises due to the larger field at the contact area [32]. It is common knowledge that the standard insulator layer at the interface, like SiO_2, is unable to fully deactivate the semiconductor surface in MIS-type structures when produced using traditional methods like thermal or sputtering techniques [33]. Nevertheless, the active dangling bonds can be reduced by implementing a special material, like an MPS structure. This leads to an increase in shunt resistance, BH, and RR, while simultaneously reducing leakage current and surface states [34–38]. Due to the intriguing physical properties exhibited by polymers or metal-doped polymers, such as being cost-effective, possessing a wide range of bandgaps and crystallinity, non-toxicity, and easy growth technologies, MPS-type structures have replaced conventional MIS structures in recent years to enhance the quality or performance of MS structures. Additionally, when subjected to an external electric field that displaces charges from their equilibrium position or captures them, resembling behavior observed in insulator materials [33,34].

In contrast to MIS-type photodiodes (PDs), the first aim of this work is to construct an MPS-type PD with a structure of Al/PVP:$ZnTiO_3$/p-Si due to the ease with which the interfacial nanocomposite layer between the metal and semiconductor may be created utilizing a straightforward spin-coating approach. When compared to traditional oxide layer materials, growing a polymer interfacial layer without/with metal and metal-oxide nanoparticles dopant at the M/S interface is easier and cheaper. Especially, low molecular weight, low cost, flexibility, and lightness are some features that make polymeric or organic interfacial layers advantageous [9–11]. On the other hand, once these polymers are doped by metal, metal-oxide, and graphene nanoparticles, they reveal interesting electrical/dielectric features such as high dielectric strength and electrons/holes storage capability because of their OH groups and H-bonding formation [16,17]. Then, the primary electronic properties of the fabricated MPS-type PD are examined by measuring the I–V characteristics in the dark and under a range of light intensities of 450–750 mW/cm^2 at room temperature. The resistance and interface state profiles of the prepared sample at each illumination intensity are determined as a function of bias voltage and the energy, respectively. Next, the values of open-circuit voltage (V_{oc}), short circuit current (I_{sc}), filling factor (FF), and efficiency (η) are obtained under different illumination intensities. Eventually, the created MPS-type PD's photo-response is compared to the PDs that were previously introduced, and its performance is thoroughly analyzed.

2. Experimental details

ROYALEX and Merck Companies supplied $TiCl_4$ (99 %) and Zn $(CH_3COO)_2.2H_2O$ (99 %), respectively. TiO_2 nano-powders were made, as stated in our published paper Ref. [35]. To make the $ZnTiO_3$ nanostructures, we first prepared 20^{cc} each of 0.2 M $Zn(CH_3CO_2)_2$, 0.2 M NaOH, and 0.1 M TiO_2 solutions in separate beakers before starting the synthesis of the $ZnTiO_3$ nanostructures. Drop by drop, under ultrasonic irradiation, and at room temperature, the solutions of TiO_2 and NaOH were added to the $Zn(CH_3CO_2)_2$ solution. The outcome was then put into a microwave device and treated to 800 W of microwave radiation for 10 min. After that, the product was dried at room temperature after being rinsed during centrifugation. The resultant nano-powder was then annealed for 2 h at 700 °C. The 10^{cc} PVP solution was mixed with 0.1 g of $ZnTiO_3$ nano-powder to create the PVP:$ZnTiO_3$ nanocomposite. The $ZnTiO_3$ nanoparticles were dispersed in a PVP solution while being exposed to ultrasonic radiation.

In this present study, the structure of Al/PVP:$ZnTiO_3$/p-Si was grown on the B-doped (p-Si) wafer with 1–10 Ω cm^{-1} resistivity, (100) orientation, ~300 μm thickness, 2″ diameter, and one-side polished. Firstly, p-Si wafer was ultrasonically cleaned in a chemical solution of (HF + $10H_2O$) for 5 min and then rinsed in deionize water to remove any native oxide layer from the surface of wafer. After that, it was rinsed in the (H_2SO_4:H_2O_2:H_2O)/(5:1:1) and (HCl:H_2O)/(1:1) chemical solutions for 4 min and, then it was dipped into high pure deionized water (DW) with 18 MΩ cm^{-1} resistivity and dried by high-pure N_2 gas. Secondly, the whole back-side of the p-Si wafer was thermally evaporated with 150 nm thick Al (99.999 %) at 1μTorr and, then it was annealed at 500 °C for 5 min in an N_2 atmosphere to get good or low-resistivity back ohmic contact. Thirdly, the prepared solution of PVP:$ZnTiO_3$ was immediately spun-coated on the other side of the wafer at 3000 rpm for 1 min. The thickness of the interfacial layer has been estimated by the measured

capacitance of the interfacial layer to be 60 nm. Finally, circular Al rectifier or Schottky contacts with 1.2 mm diameter and 150 nm thickness were also thermally evaporated in the same high vacuum metal evaporation system. The thickness of ohmic and rectifier metal contacts was controlled by using a quartz thickness meter.

Fig. 1 shows schematically the MPS-type PD and its energy-bandgap diagram. The XRD pattern, SEM image, and UV–Vis absorption spectra of $ZnTiO_3$ nanostructures was given in our previous study [39]. The highest and lowest occupied molecular orbitals (HOMO, LUMO) energies, as well as the energy gap between them for the PVP polymer, was also calculated in the same paper. It is necessary to mention that the Keithley 4200 current/voltage source was used to measure the I–V characteristics of the fabricated device in the dark and under illumination at room temperature. Meanwhile, a Newport-Oriel 69,931 whose power is in range 400–900 mW was employed to illuminate the MPS-type PD in solar spectrum.

3. Results and discussion

Fig. 2a displays semilogarithmic profiles of the I–V characteristics for the MPS-type PD over a wide voltage range (±3 V) at specific illumination intensities (450–750 mW/cm^2). The profiles of lnI-V have been extracted from the I–V values at lower positive voltages that had a good rectifying behavior. At lower positive voltages, the curves exhibit acceptable linear behavior; however, at higher forward bias voltages, the PVP:$ZnTiO_3$ nanocomposite at the M/S interface and R_s produce bendings. To analyze the proficiency of the fabricated silicon-based MPS-type PD under normal forward bias conditions I–V range, the theory of thermionic emission (TE) is used. As a result, if the structure has sufficient high R_s and $n > 1$, the relation for (V>3kT/q) is given by Refs. [36,37]:

$$I = I_0\left[\exp\left(\frac{q(V_F - IR_s)}{nkT}\right) - 1\right] \quad (1)$$

with I_0 and IR_s being the saturation-current and the voltage across the R_s of the structure, respectively. The quantity of I_0 is defined as follows [38]:

$$I_0 = AA^*T^2 \exp\left(-\frac{q\varphi_{B0}}{kT}\right) \quad (2)$$

where A and A* denote the contact space and the Richardson constant, respectively. The lnI-V graphs' intersection points with the axis of lnI at the linear parts, which were established in the voltage range of roughly 0.24–0.38 V at both dark and under illumination conditions, were used to calculate the I_0 values. The value of BH at V = 0 is then obtained utilizing the area (=7.85 × 10^{-3} cm^2) as [38]:

$$\varphi_{B0} = \frac{kT}{q}\ln\left(\frac{AA^*T^2}{I_0}\right) \quad (3)$$

The slop of the linear segments in the lnI-V plots by considering tanθ = dln(I)/dV and kT/q are also utilized to calculate the ideality factor of the manufactured MPS-type PD as [38,39]:

$$n = \frac{q}{kT}\left(\frac{dV_F}{d(\ln I_F)}\right) \quad (4)$$

It is worth mentioning that the forward and reverse bias regions of the I–V characteristics can also be employed to determine the values of R_s and R_{sh}, respectively. These two characteristics have a significant impact on the effectiveness of PDs and SCs. Ohm's Law may be used to determine how the structure's resistance (R_i) changes with voltage ($R_i = V_i/I_i$); hence, the values of R_s and R_{sh} are corresponding to high forward and low reverse bias voltages, respectively [39].

The voltage-dependent R_i curves of the prepared PD for different illumination powers are consequently represented in Fig. 2b. It is obvious from Fig. 2b, as the illumination power increased, the photocurrent increased as well, which led to a fall in the R_s values. From the measurements and the calculations, the vital diode parameters (I_0, n, Φ_{B0}, R_{sh}, and R_s) are found and presented in Table 1. According to standard TE theory, the value of n is supposed to be equal to unity in an ideal case, but a high value of n means a deviation from TE theory. Both n and BH values for MS- and MPS-type structures may be quite a function of forward-bias voltage. Besides, the structure may contain many lower barriers/paths at around mean BH that many electrons with low energies can pass through these lower barriers, leading to increasing the values of current and n. As seen, when the illumination power increased,

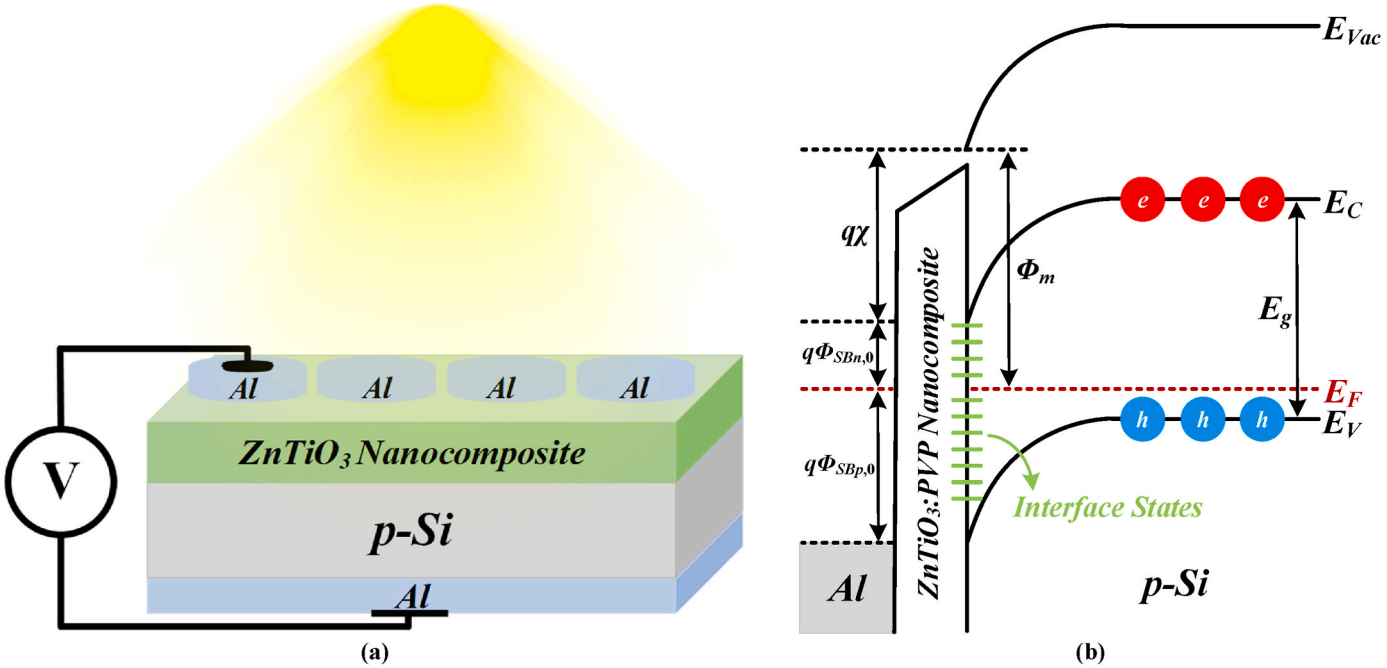

Fig. 1. Schematic of (a) the structure and (b) the energy-band diagram of the MPS-type PD.

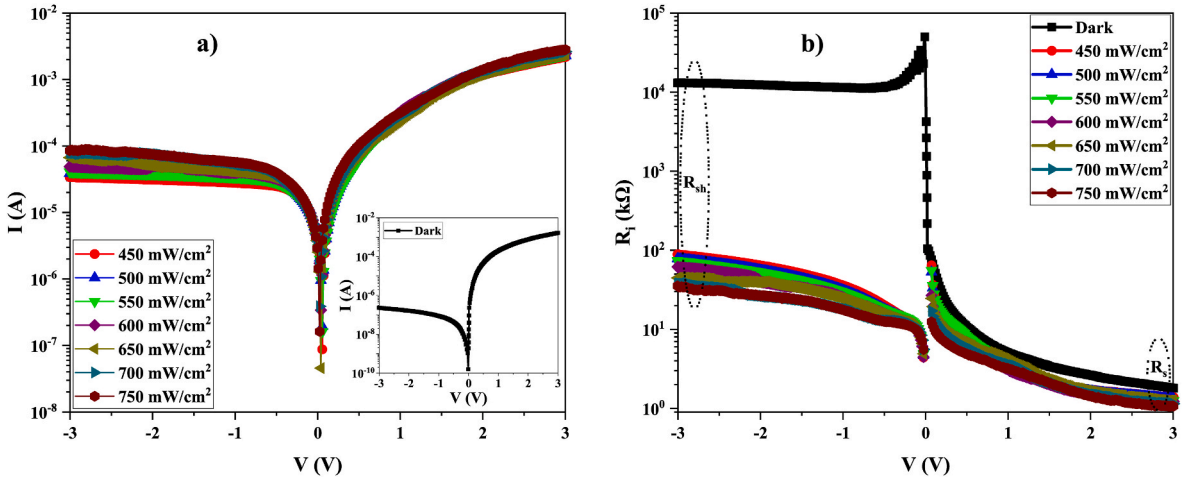

Fig. 2. The semilogarithmic profiles of (a) I–V and (b) R_i-V of the prepared Schottky PD in dark and under illumination.

Table 1
Dependence of the main electronic factors of the fabricated Schottky PD on the illumination.

P (mW/cm^2)	I_0 (μA)	n	Φ_{B0} (eV)	R_{sh} (kΩ)	R_s (kΩ)
0	2.22	5.81	0.687	13,905	1.80
450	3.14	6.93	0.673	88.57	1.38
500	3.84	7.12	0.668	77.93	1.32
550	4.98	7.38	0.661	73.62	1.25
600	6.72	7.49	0.653	61.45	1.22
650	8.05	7.82	0.649	44.73	1.18
700	8.63	7.92	0.647	37.57	1.14
750	11.5	8.09	0.639	35.37	1.06

the values of I_0 and n rise while Φ_{B0}, R_{sh}, and R_s values decline. The increase of the photocurrent at both voltage regions causes this behavior.

The three most crucial electrical parameters, i.e., n, Φ_{B0}, and R_s, can be determined using a variety of methods found in the literature as standard TE theory, Norde, and Cheung functions, but each one corresponds to a various voltage region. The real value of Rs can be obtained by various calculation methods from the forward bias I–V data, such as Ohm's law, Norde, and Cheung's function, while the nature of them may be different due to the chosen or studied bias voltage. For example, according to Ohm's law, the real value of Rs in electronic devices corresponds to higher forward-bias voltages, while Norde and Cheung's functions are suitable only if the ln(I)–V curve has a clear linear range. In this case, the accuracy and reliability of calculated electronic parameters are discussed.

After determining these parameters using the three alternative approaches, the results are compared. If the forward bias lnI-V profiles do not contain sufficient linear regions, the last two techniques are typically employed. When $n > 1$, the F(V) function for the modified Norde technique is given by Ref. [40]:

$$F(V) = \frac{V}{\gamma} - \frac{kT}{q}\left[\ln\left(\frac{I(V)}{AA^*T^2}\right)\right] \tag{5}$$

with γ being a positive integer with no dimensions greater than n. As a result, the values of V_{min} and I_{min}, which are the voltage-dependent profiles of F(V) function as shown in Fig. 3, can be used to calculate the Φ_{B0} and R_s quantities as [40]:

$$\Phi_{B0} = F(V_{min}) + \frac{V_{min}}{\gamma} - \frac{kT}{q} \tag{6a}$$

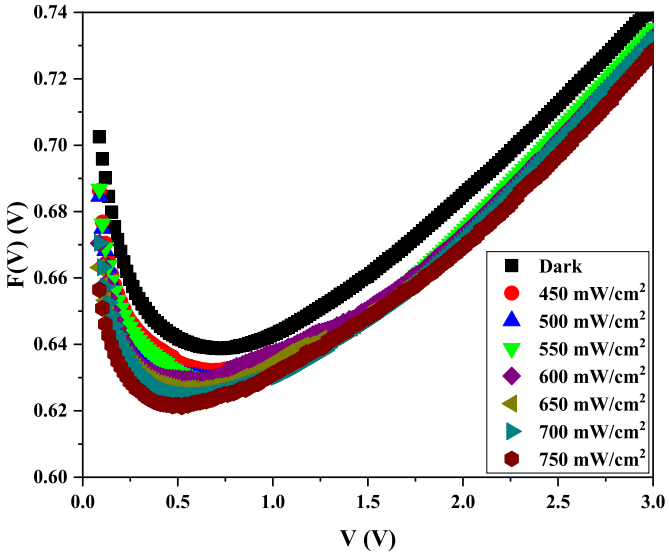

Fig. 3. The illumination-dependent F(V)–V profiles of the MPS-type PD.

$$R_s = \frac{kT}{q}\frac{(\gamma - n)}{I_{min}} \tag{6b}$$

Table 2 contains the computed Φ_{B0} and R_s quantities from Equations (6a) and (6b). Similar to the TE theory, the amounts of Φ_{B0} and R_s rise as illumination power decreases.

By applying the following two equations as Cheung's functions, it is also possible to get the fundamental values of n, Φ_{B0}, and R_s [41]:

$$\frac{dV}{d(lnI)} = IR_s + \left(\frac{nkT}{q}\right) \tag{7a}$$

$$H(I) = V - \frac{nkT}{q}\ln\left(\frac{I}{AA^*T^2}\right) = IR_s + n\Phi_{B0} \tag{7b}$$

Fig. 4(a and b) shows the electronic current-dependent graphs of dV/dln(I) and H(I) for the MPS-type PD at both dark and illumination conditions that were created using Equations (7a) and (7b). According to Equation (7a), the quantities of R_s and n were determined by analyzing the gradients and intersection of the profiles of dV/dln(I)–I. Subsequently, by plotting H(I)–I graphs with the use of these n values in Equation (7b), the slope and intercept of the graphs are utilized to compute Φ_{B0} and R_s.

Table 2
Electrical parameters of the MPS-type PD in dark and under illumination computed by different methods.

Power (mW/cm^2)	Φ_{B0} (eV)			I_0 (μA)	R_s (kΩ)				R_{sh} (kΩ)	n		$N_{ss} \times 10^{13}$ (eV^{-1} cm^{-2})
	TE	Norde	H(I)		TE	Norde	H(I)	dV/dln(I)		TE	dV/dln(I)	
0	0.682	0.672	0.707	2.22	1.80	1.80	1.62	1.78	13,905	5.81	6.72	1.69
450	0.673	0.667	0.675	3.14	1.38	1.37	1.24	1.31	88.5	6.93	6.98	1.65
500	0.669	0.664	0.634	3.84	1.32	1.31	1.23	1.29	77.9	7.12	7.26	1.64
550	0.661	0.659	0.632	4.98	1.25	1.24	1.21	1.27	73.6	7.38	7.48	1.63
600	0.653	0.654	0.615	6.72	1.22	1.21	1.16	1.25	61.5	7.49	7.62	1.63
650	0.649	0.650	0.598	8.05	1.18	1.18	1.13	1.19	44.7	7.82	7.84	1.63
700	0.646	0.647	0.584	8.63	1.14	1.12	1.08	1.17	37.6	7.92	7.96	1.62
750	0.639	0.637	0.580	11.5	1.07	1.05	1.02	1.12	35.4	8.08	8.08	1.61

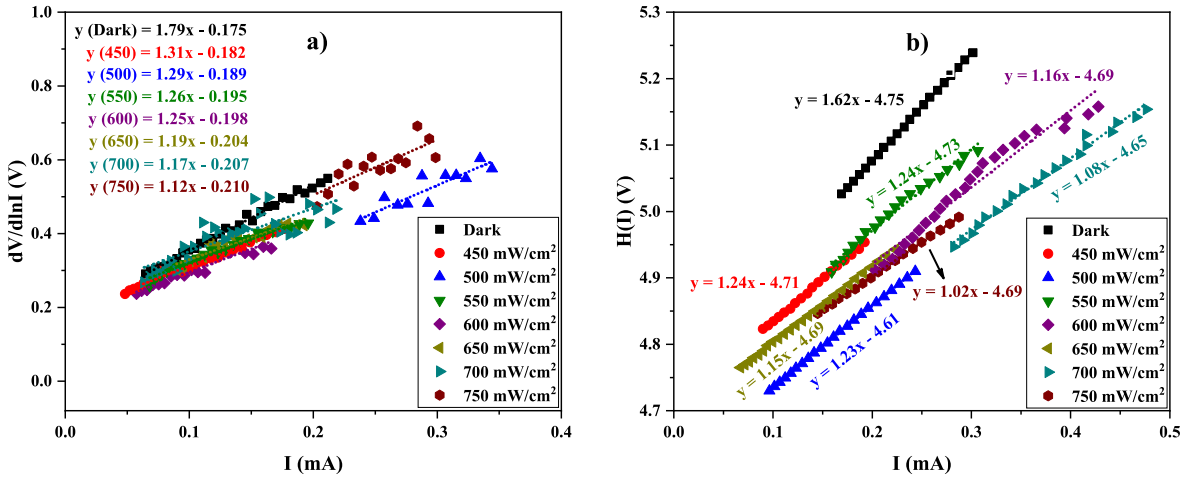

Fig. 4. The (a) dV/dlnI and (b) H(I) profiles versus I of the MPS-type PD in dark and under illumination.

In the present study, the primary electrical parameters of n, Φ_{B0}, and R_s were calculated by standard TE theory, Norde, and Cheung's functions. Cheung's methods allow us to obtain these essential electrical parameters from the region where the ln(I)–V graph is linear. According to Card and Rhoderick, both n and BH values depend on voltage, and they can be quite different from just the linear part of the ln(I)–V plot and the fitted it's to zero voltage (I_0). In other words, the voltage dependence of these factors and calculation techniques may be the reason for the observed disparities. It is necessary to note that the TE theory is valid in the moderate forward bias voltages while Cheung functions are correct at high forward bias voltages.

It is well known that the existence of both R_s and N_{ss} may considerably influence the I–V curve of the MS- and MPS-type structures at the forward bias range. The R_s are rooted from the ohmic/rectifier contacts, the used probe wires to the gate, the bulk-resistivity of the semiconductor, and in-homogeneities of doping-atoms in the semiconductor, the native or deposited interlayer at the M/S interface [1,4,6]. The formation of N_{ss} usually originates from the interruption of the periodic-lattice structure of the semiconductor surface, cleaning and surface preparation, some impurities in the semiconductor, and organic pollution in the grown environment [6]. The presence of N_{ss} at the M/S interface is also more effective on the optical response of the MPS-type PD, and it has a substantial impact on how well electrical devices like MIS, MPS-type PDs, and SCs work and are made. The changes in energy-dependent N_{ss} are thus calculated based on the equations provided below, derived from the positive values of current and voltage, considering the voltage-dependent Φ_{B0} and n(V) [42]:

$$E_{ss} - E_v = q(\Phi_e - V) \tag{8a}$$

$$\Phi_e - \Phi_{B0} = \beta(V - IR_s) = \left(1 - \frac{1}{n(V)}\right)(V - IR_s) \tag{8b}$$

$$N_{ss}(V) = \frac{1}{q}\left[\frac{\varepsilon_i}{\delta}(n(V) - 1) - \frac{\varepsilon_s}{W_D}\right] \tag{8c}$$

In Equations (8a)-(8c), ε_i is the interfacial layer's dielectric constant, ε_s is the semiconductor's dielectric, W_D is the depletion layer's thickness, and δ_i is the interfacial layer's thickness. Fig. 4 illustrates the obtained value of N_{ss} as a function of energy for each illumination intensity that is approximately 10^{13}/(eV.cm^2).

The realignments and reorganizations of N_{ss} in the presence of illumination and an electric field are due to the observed differences or positions in N_{ss}. As seen in Fig. 5, the N_{ss} quantities increase from close to the semiconductor's intermediate bandgap towards the edge of the valence band (E_v), changing from 1.0 × 10^{11} to 1.7 × 10^{13}/(eV.cm^2). Practically for each illumination intensity. Rearranging and reorganizing N_{ss} in an electric field under illumination causes this increase. The energy states or traps may serve as a recombination center, capturing and releasing electrons depending on their lifetime and the illumination's intensity. Therefore, the illumination-induced N_{ss} are able to be reordered and restructured under an electric field, and their position shifts towards the top of the valence band.

To compare the results obtained by TE theory, Norde and Cheung functions, the essential electrical characteristics (n, Φ_{B0}, and R_s) of the MPS-type PD are reported in Table 2. The values of Φ_{B0}, N_{ss}, R_s, and R_{sh} reduce by increasing the illumination power while the I_0 and n quantities raise. Although the results are in good agreement with each other, some differences are observed owing to different approaches used in these methods to derive the voltage-dependent parameters. The value of n reflects the quality prepared PD, and it is expected almost unity in the ideal case, but as can be seen from [$n = 1+d_i/\varepsilon_s(\varepsilon_s/W_d + qN_{ss})$], it may be considerably deviated from unity in the application due to the existence interlayer, its thickness (d_i) and permittivity (ε_i), the doping level of donor or acceptor atoms, depletion layer width (W_d), a particular

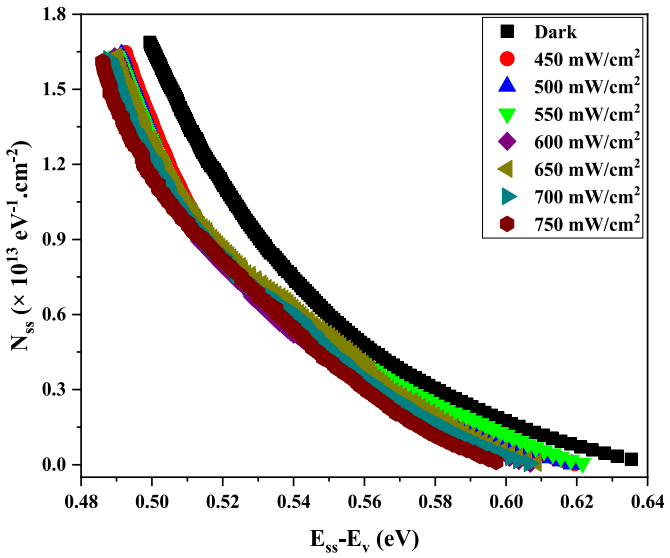

Fig. 5. The energy-dependent N_{ss} profiles of the MPS-type PD in dark and under illumination.

distribution of N_{ss} at interlayer/semiconductor interface with energy states in the band gap of the semiconductor, image-force lowering of BH, generation-recombination electronic charges, tunneling via surface–states, and barrier inhomogeneities at the M/S interface [1–6,26,27].

Fig. 6a shows the variations of the barrier height (Φ_{B0}) of the MPS-type PD as a function of the illumination intensity (P). Given the equation $\Phi_{B0}(P) = \Phi_{B0}$-$\alpha P = (-1.11P + 0.723)$ derived from the plot slope of Fig. 6b, there is also a relationship between Φ_{B0} and P. In this equation, α denotes the illumination coefficient that is obtained as $\alpha = d\Phi_{B0}/dP = -1.11$. Moreover, Fig. 6b shows the changes of the barrier height (Φ_{B0}) of the MPS-type PD in terms of the ideality factor (n). As seen, the equation of $\Phi_{B0}(n) = (-0.021n + 0.814)$ eV states that there is a relationship between Φ_{B0} and n based on the plot slope. As a result, the value of Φ_{B0} is determined as 0.793 eV for n = 1 (ideal case). The presence of the interfacial layer of PVP:$ZnTiO_3$, its thickness, the width of the depletion layer (W_d), the concentration of donor atoms used for doping (N_d), N_{ss}, and barrier inhomogeneity are all factors that contribute to the n quantities estimated for different illumination being larger than the value in the ideal situation [43,44].

When electrons presented at the interface traps/states or the valence band acquire enough energy through exposure to light exceeding the band gap (E_g), they can transition to the conduction band or become trapped at another location, leading to the generation of a photocurrent. Regardless of the intensity of the illumination, the value of the electric current at the zero voltage and the voltage value at the zero current are known as I_{sc} and V_{oc}, respectively. Fig. 7a represents the efficiency I–V profiles for each illumination that may be used to calculate the V_{oc}, I_{sc}, FF, and efficiency (η) of the MPS-type PD. Therefore, using the effective contact area and illumination intensity (P_{in}), the yield of the MPS-type PD could also be given by Refs. [44,45]:

$$FF = [(V_m I_m) / (V_{oc} I_{sc})] \tag{9a}$$

$$\eta = FF \times [(V_{oc} I_{sc}) / P_{in} A] \tag{9b}$$

At each illumination intensity, V_m and I_m refer to the values of the voltage and current that correspond to the maximum power quantities of the efficiency I–V graphs. The values of V_{oc}, I_{sc}, FF, and η are discovered under different illumination powers and listed in Table 3. Because the PVP:$ZnTiO_3$ interfacial layer and R_s are present, η has a lower value.

The photo-conducting behavior causes the observation of the current in the reverse bias region. As seen in Fig. 7b, the photocurrent values (I_{ph}) increased linearly with increasing illumination power (P) for certain negative voltage values. This linear relation is provided with the power law given by Ref. [46]:

$$I_{ph} = BP^n \tag{10}$$

with B and n being a constant and an exponent. The slope of the ln(I_{ph})-ln(P) graph, which are used to calculate the value of n, changed between 0.113 and 0.850 for different bias voltages applied (−0.4 V, −0.3, −0.2, −0.1, and 0.0) [47]. Fig. 7b illustrates how the photocurrent value rises with increasing illumination intensity. Determining the ideal thickness of the absorbent layer in solar cells is therefore required. The absorbing layer causes a decreased photocurrent value when the interfacial layer's thickness is very thin. However, the thick interfacial layer causes a high series resistance and reduces photocurrent. On the other hand, by evaluating the density of photocurrent while considering the distribution of solar radiation spectrum, it is feasible to deduce the characteristic properties of solar cell efficiency for different thicknesses of the photoactive layer. This causes an increase in the V_{oc} but a drop in I_{sc} when the interfacial oxide layer thickness is increased. Therefore, to provide optimal efficiency in SCs or PDs, it is crucial to ascertain the thickness of the interfacial layer. Instead of attempting to boost battery efficiency and investigate the cause, our goal in this instance is to measure the fundamental battery characteristics that influence efficiency.

Fig. 8 demonstrates the rates of I_{ph}/I_{dark} for the fabricated MPS-type PD which determined photosensitivity (S) in the reverse bias voltage, between −3 and 0 V. The introduced Al/PVP:$ZnTiO_3$/p-Si MPS-type PD

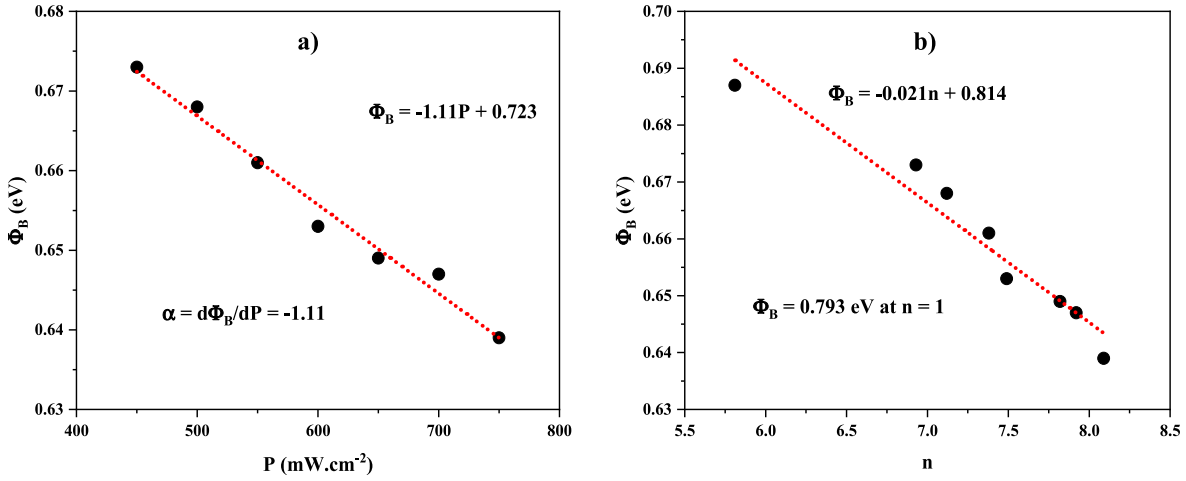

Fig. 6. The profiles of (a) Φ_B-P and (b) Φ_B-n of the MPS-type PD.

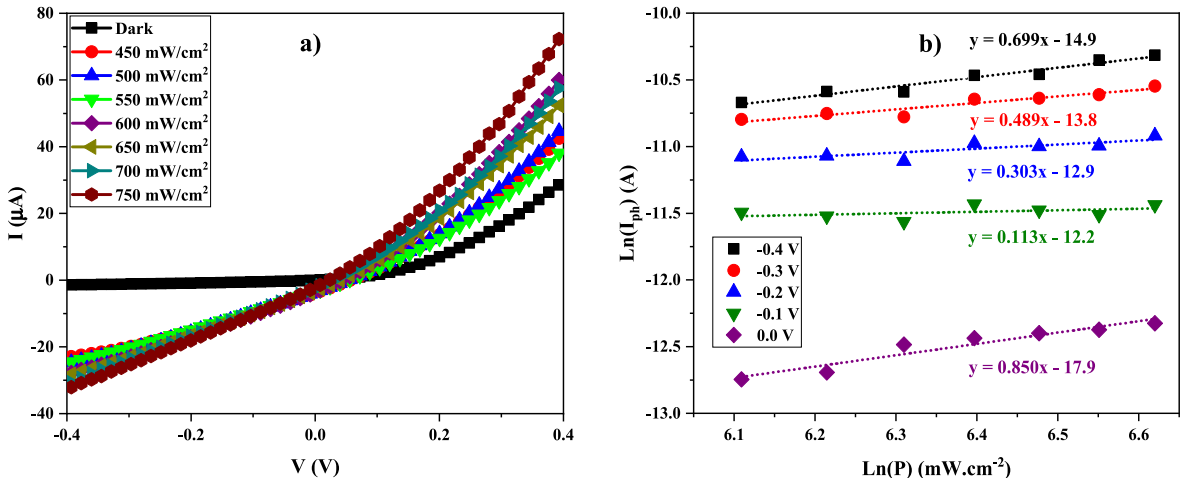

Fig. 7. The (a) efficiency I–V and (b) $Ln(I_{ph})$-Ln(P) profiles of the MPS-type PD.

Table 3
The efficiency parameters of the MPS-type PD.

P (mW/cm^2)	I_{sc} (μA)	V_{oc} (mV)	FF (%)	η (%)
450	3.92	56	37.00	2.30
500	3.6	53	42.58	2.07
550	3.5	54	42.98	1.88
600	3.6	40	56.42	1.72
650	3.15	40	64.48	1.59
700	2.80	24	120.89	1.49
750	2.15	24	157.44	1.38

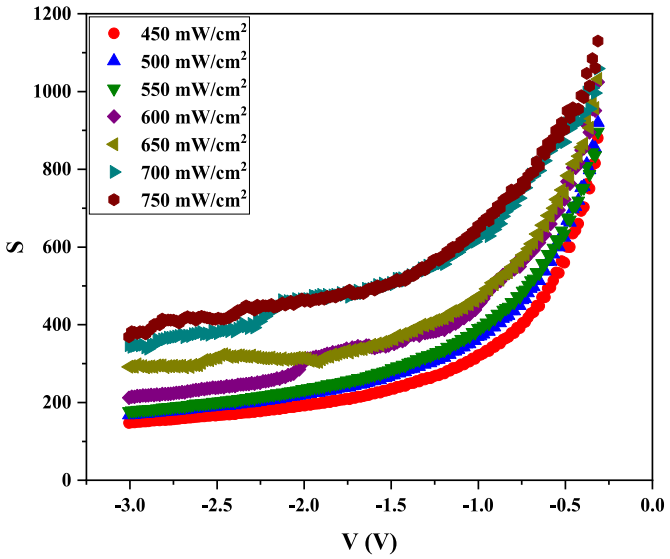

Fig. 8. The S–V profiles of the MPS-type PD under different illumination intensity.

has a strong photosensitivity in the negative/reverse bias voltage, as observed in Fig. 8 where The photosensitivity value rises in correlation with the intensity of light across all measured reverse bias voltages. Similar results for MPS-type PDs have recently been described in the literature [48–52]. The photosensitivity of the manufactured silicon-based PD presented in this work is about ~ 500 which is higher than the photosensitivity of the PD introduced in Refs. [49–51]. It must be noted that the interfacial layer's thickness, permittivity, barrier inhomogeneities at M/S interface, a unique density distribution of N_{ss} in the semiconductor's bandgap, voltage dependency, and fabrication methods can all affect the performance of PDs, leading to the differences observed in the photosensitivity values (see Fig. 8).

When a native or deposited insulator/polymer interlayer exists between metal and semiconductor, MS contacts/diodes convert to the MIS/MPS type diodes. The existence of such an interlayer gives them the properties of a capacitor, which stores more electric charges/energy, possessing the dielectric properties [9–11,24]. Unless a particular fabrication of these structures, many surface/interface states may occur at the interlayer/semiconductor interface with energy states in the semiconductor band gap (E_g), depending on the chemical composition of the interface [9–11,24]. Therefore, today, there are many attempts to improve the performance of both MS and MIS structures and supply a continuous control of the BH using pure or doped polymer interlayer [53–55]. For instance, Altındal Yerişkin et al. [53] recently manufactured both MS (Au/n-Si) and MPS (Au/PVA:Graphene/n-Si) structures on the same n-Si crystal at identical conditions, and they are indicated that both values of rectification ratio (RR at ±5 V) and N_{ss} of MPS structure is 493 times higher and 93 lower than the MS one, respectively. Reddy et al. [34] showed that the N_{ss} value of the MPS (Au/PVDF/n-InP) structure is one order lower than the MS (Au/n-InP) structure due to the dangling bonds saturation by using this polymer interfacial layer. Çiçek et al. [54] observed that an increase in RR and R_{sh} and a decrease in N_{ss} and R_s for the Au/PVA:Graphene/n-GaAs structure.

4. Conclusion

Instead of manufacturing MS-type SDs using an insulator thin film developed using a conventional process, a spin-coated PVP:$ZnTiO_3$ nanocomposite interfacial layer was used to fabricate a Schottky PD in this research. By measuring I–V characteristics of the Schottky PD exposed with illuminations in the range of 450–750 mW/cm^2 at room temperature, certain crucial electrical parameters were then acquired. To determine the voltage dependence of fundamental electrical features of the considered Schottky PD at each illumination intensity, the Φ_{B0}, n, and R_s were computed using the TE theory, Norde, and Cheung's functions. It was seen that the quantity of Φ_{B0} and R_s are decreased by increasing the illumination power while the value of n rises. Additionally, the energy-dependent N_{ss} quantities were measured at the dark and each illumination intensity. According to the experimental findings, the value of Φ_{B0} declines linearly with increasing P and n, with $\Phi_{B0}(P) = (-1.11P + 0.723)$ eV and $\Phi_{B0}(n) = (-0.021n + 0.814)$ eV, giving the illumination coefficient ($\alpha = -1.11$) and Φ_{B0} (=0.793) at ideal case (n = 1). The values of V_{oc}, I_{sc}, FF, and η were obtained at different illumination powers. It was found that the efficiency is maximum at the lowest illumination intensity (450 mW/cm^2). An increase in I_{ph} was also seen because of the e^--h^+ pairs that form at negative bias region by rising

power of illumination. An excellent linear behavior was visible at various applied voltages in the ln(I_{ph})-ln(P) profiles. Their slopes varied from 0.113 to 0.850, showing empty trap levels-levels devoid of charges-have a low density. The photosensitivity (S) of the silicon-based PD developed in this work is about 500, higher than some PDs introduced in the literature. These findings suggest that the manufactured MPS-type PD with a structure of Al/PVP:$ZnTiO_3$/p-Si can be employed in SCs and photovoltaics applications.

CRediT authorship contribution statement

Ali Barkhordari: Conceptualization, Data curation, Formal analysis, Investigation, Writing – original draft, Methodology. **Hamid Reza Mashayekhi:** Supervision, Writing – review & editing. **Pari Amiri:** Supervision, Writing – review & editing. **Şemsettin Altındal:** Supervision, Writing – review & editing. **Yashar Azizian-Kalandaragh:** Project administration, Supervision, Writing – review & editing.

Declaration of competing interest

The authors declare that they have no known competing financial interests or personal relationships that could have appeared to influence the work reported in this paper.

Data availability

Data will be made available on request.

References

[1] M. Sharma, S.K. Tripathi, Analysis of interface states and series resistance for Al/PVA: n-CdS nanocomposite metal–semiconductor and metal–insulator–semiconductor diode structures, Appl. Phys. A 113 (2013 Nov) 491–499.

[2] F. Aslan, H. Esen, F. Yakuphanoglu, Electrical and fotoconducting characterization of Al/coumarin: ZnO/Al novel organic-inorganic hybrid photodiodes, J. Alloys Compd. 789 (2019 Jun 15) 595–606.

[3] P. Kumar, S.C. Jain, V. Kumar, S. Chand, R.P. Tandon, Effect of illumination on the space charge limited current in organic bulk heterojunction diodes, Appl. Phys. A 94 (2009 Feb) 281–286.

[4] S.M. Sze, Y. Li, K.K. Ng, Physics of Semiconductor Devices, John wiley & sons, 2021 Mar 19.

[5] J.H. Werner, H.H. Güttler, Barrier inhomogeneities at Schottky contacts, J. Appl. Phys. 69 (3) (1991 Feb 1) 1522–1533.

[6] E.H. Nicollian, J.R. Brews, MOS (Metal Oxide Semiconductor) Physics and Technology, John Wiley & Sons, 2002 Nov 21.

[7] M.S. Reddy, P.T. Puneetha, Y.W. Lee, S.H. Jeong, C. Park, Effect of illumination and frequency dependent series resistance and interface state densities on the electrical properties of DNA-CTMA/p-GaN bio-hybrid Schottky photodiode, Polym. Test. 59 (2017 May 1) 107–112.

[8] H.G. Çetinkaya, Ş. Altındal, I. Orak, I. Uslu, Electrical characteristics of Au/n-Si (MS) Schottky diodes (SDs) with and without different rates (graphene+ Ca 1.9 Pr 0.1 Co 4 O x-doped poly (vinyl alcohol)) interfacial layer, J. Mater. Sci. Mater. Electron. 28 (2017 Jun) 7905–7911.

[9] S. Demirezen, S. Altındal Yerişkin, A detailed comparative study on electrical and photovoltaic characteristics of Al/p-Si photodiodes with coumarin-doped PVA interfacial layer: the effect of doping concentration, Polym. Bull. 77 (1) (2020 Jan) 49–71.

[10] M. Siva Pratap Reddy, K. Sreenu, V. Rajagopal Reddy, C. Park, Modified electrical properties and transport mechanism of Ti/p-InP Schottky structure with a polyvinylpyrrolidone (PVP) polymer interlayer, J. Mater. Sci. Mater. Electron. 28 (2017 Mar) 4847–4855.

[11] P. Singh, A. Kumar, D. Kaur, ZnO nanocrystalline powder synthesized by ultrasonic mist-chemical vapour deposition, Opt. Mater. 30 (8) (2008 Apr 1) 1316–1322.

[12] P. Singh, A. Kumar, D. Kaur, Substrate effect on texture properties of nanocrystalline TiO2 thin films, Phys. B Condens. Matter 403 (19–20) (2008 Oct 1) 3769–3773.

[13] N. Wang, X. Li, Y. Wang, Y. Hou, X. Zou, G. Chen, Synthesis of ZnO/TiO2 nanotube composite film by a two-step route, Mater. Lett. 62 (21–22) (2008 Aug 15) 3691–3693.

[14] B.B. Rao, Zinc oxide ceramic semi-conductor gas sensor for ethanol vapour, Mater. Chem. Phys. 64 (1) (2000 Mar 31) 62–65.

[15] Y. Yoshino, T. Makino, Y. Katayama, T. Hata, Optimization of zinc oxide thin film for surface acoustic wave filters by radio frequency sputtering, Vacuum 59 (2–3) (2000 Nov 1) 538–545.

[16] S. Jäger, B. Szyszka, J. Szczyrbowski, G. Bräuer, Comparison of transparent conductive oxide thin films prepared by ac and dc reactive magnetron sputtering, Surf. Coating. Technol. 98 (1–3) (1998 Jan 1) 1304–1314.

[17] R.W. Birkmire, E. Eser, Polycrystalline thin film solar cells: present status and future potential, Annu. Rev. Mater. Sci. 27 (1) (1997 Aug) 625–653.

[18] D.C. Look, Recent advances in ZnO materials and devices, Mater. Sci. Eng. B 80 (1–3) (2001 Mar 22) 383–387.

[19] A.B. Bodade, A.M. Bende, G.N. Chaudhari, Synthesis and characterization of CdO-doped nanocrystalline ZnO: TiO2-based H2S gas sensor, Vacuum 82 (6) (2008 Feb 19) 588–593.

[20] X. Zhang, F. Zhang, K.Y. Chan, The synthesis of Pt-modified titanium dioxide thin films by microemulsion templating, their characterization and visible-light photocatalytic properties, Mater. Chem. Phys. 97 (2–3) (2006 Jun 10) 384–389.

[21] H.T. Kim, S. Nahm, J.D. Byun, Y. Kim, Low-fired (Zn, Mg) TiO3 microwave dielectrics, J. Am. Ceram. Soc. 82 (12) (1999 Dec) 3476–3480.

[22] H. Obayashi, Y. Sakurai, T. Gejo, Perovskite-type oxides as ethanol sensors, J. Solid State Chem. 17 (3) (1976 Mar 1) 299–303.

[23] Y. Shimizu, H. Komatsu, S. Michishita, N. Miura, N. Yamazo, Sensing characteristics of hydrogen peroxide sensor using carbon-based electrode loaded with perovskite-type oxide, Sensor. Actuator. B Chem. 34 (1–3) (1996 Aug 1) 493–498.

[24] S.F. Wang, M.K. Lü, F. Gu, C.F. Song, D. Xu, D.R. Yuan, G.J. Zhou, Y.X. Qi, Photoluminescence characteristics of Pb2+ ion in sol–gel derived ZnTiO3 nanocrystals, Inorg. Chem. Commun. 6 (2) (2003 Feb 1) 185–188.

[25] M. Gabrovska, R. Edreva-Kardjieva, K. Tenchev, P. Tzvetkov, A. Spojakina, L. Petrov, Effect of Co-content on the structure and activity of Co–Al hydrotalcite-like materials as catalyst precursors for CO oxidation, Appl. Catal. Gen. 399 (1–2) (2011 May 31) 242–251.

[26] Y. Gui, S. Li, J. Xu, C. Li, Study on TiO2-doped ZnO thick film gas sensors enhanced by UV light at room temperature, Microelectron. J. 39 (9) (2008 Sep 1) 1120–1125.

[27] S.F. Wang, F. Gu, M.K. Lü, C.F. Song, D. Xu, D.R. Yuan, S.W. Liu, Photoluminescence of sol–gel derived ZnTiO3: Ni2+ nanocrystals, Chem. Phys. Lett. 373 (1–2) (2003 May 13) 223–227.

[28] F.H. Dulln, D.E. Rase, Phase equilibria in the system ZnO-TiO2, J. Am. Ceram. Soc. 43 (3) (1960 Mar) 125–131.

[29] U. Steinike, B. Wallis, Formation and structure of Ti-Zn-oxides, Cryst. Res. Technol. 32 (1) (1997) 187–193.

[30] B.L. Sharma (Ed.), Metal-semiconductor Schottky Barrier Junctions and Their Applications, Springer Science & Business Media, 2013 Nov 11.

[31] M. Siva Pratap Reddy, K. Sreenu, V. Rajagopal Reddy, C. Park, Modified electrical properties and transport mechanism of Ti/p-InP Schottky structure with a polyvinylpyrrolidone (PVP) polymer interlayer, J. Mater. Sci. Mater. Electron. 28 (2017 Mar) 4847–4855.

[32] A.D. Tataroğlu, O. Dayan, N. Özdemir, Z. Serbetci, A.A. Al-Ghamdi, A. Dere, F. El-Tantawy, F. Yakuphanoglu, Single crystal ruthenium (II) complex dye based photodiode, Dyes Pigments 132 (2016 Sep 1) 64–71.

[33] H.G. Çetinkaya, Ş. Altındal, I. Orak, I. Uslu, Electrical characteristics of Au/n-Si (MS) Schottky diodes (SDs) with and without different rates (graphene+ Ca 1.9 Pr 0.1 Co 4 O x-doped poly (vinyl alcohol)) interfacial layer, J. Mater. Sci. Mater. Electron. 28 (2017 Jun) 7905–7911.

[34] V.R. Reddy, Electrical properties of Au/polyvinylidene fluoride/n-InP Schottky diode with polymer interlayer, Thin Solid Films 556 (2014 Apr 1) 300–306.

[35] A. Barkhordari, S. Özçelik, Ş. Altındal, G. Pirgholi-Givi, H. Mashayekhi, Y. Azizian-Kalandaragh, The effect of PVP: $BaTiO_3$ interlayer on the conduction mechanism and electrical properties at MPS structures, Phys. Scripta 96 (8) (2021 May 26), 085805.

[36] L. Hou, Y.D. Hou, M.K. Zhu, J. Tang, J.B. Liu, H. Wang, H. Yan, Formation and transformation of ZnTiO3 prepared by sol–gel process, Mater. Lett. 59 (2–3) (2005 Feb 1) 197–200.

[37] A. Barkhordari, S. Özçelik, G. Pirgholi-Givi, H.R. Mashayekhi, Ş. Altındal, Y. Azizian-Kalandaragh, Dielectric properties of PVP: BaTiO3 interlayer in the Al/PVP: BaTiO3/P-Si structure, Silicon 14 (10) (2022 Jul) 5437–5443.

[38] Z. Durmus, A. Durmus, H. Kavas, Synthesis and characterization of structural and magnetic properties of graphene/hard ferrite nanocomposites as microwave-absorbing material, J. Mater. Sci. 50 (3) (2015 Feb) 1201–1213.

[39] A. Barkhordari, H.R. Mashayekhi, P. Amiri, Ş. Altındal, Y. Azizian-Kalandaragh, Role of graphene nanoparticles on the electrophysical processes in PVP and PVP: ZnTiO3 polymer layers at Schottky diode (SD), Semicond. Sci. Technol. 38 (7) (2023 May 18), 075002.

[40] H. Norde, A modified forward I-V plot for Schottky diodes with high series resistance, J. Appl. Phys. 50 (7) (1979 Jul) 5052–5053.

[41] Ş. Altındal, A. Barkhordari, S. Özçelik, G. Pirgholi-Givi, H.R. Mashayekhi, Y. Azizian-Kalandaragh, A comparison of electrical characteristics of Au/n-Si (MS) structures with PVC and (PVC: Sm2O3) polymer interlayer, Phys. Scripta 96 (12) (2021 Oct 19), 125838.

[42] H.C. Card, E.H. Rhoderick, Studies of tunnel MOS diodes I. Interface effects in silicon Schottky diodes, J. Phys. Appl. Phys. 4 (10) (1971 Oct 1) 1589.

[43] R.K. Gupta, K. Ghosh, P.K. Kahol, Fabrication and characterization of NiO/ZnO p–n junctions by pulsed laser deposition, Phys. E Low-dimens. Syst. Nanostruct. 41 (4) (2009 Feb 1) 617–620.

[44] İ. Dökme, Ş. Altindal, İ. Uslu, The effects of temperature, radiation, and illumination on current–voltage characteristics of Au/PVA (Co, Zn-doped)/n-Si Schottky diodes, J. Appl. Polym. Sci. 125 (2) (2012 Jul 15) 1185–1192.

[45] A. Dere, B. Coskun, A.D. Tataroğlu, A.G. Al-Sehemi, A.A. Al-Ghamdi, H.M. Alateeq, R. Qindeel, W.A. Farooq, F. Yakuphanoglu, Boron doped graphene based linear dynamic range photodiode, Phys. B Condens. Matter 545 (2018 Sep 15) 86–93.
[46] B.P. Rand, J. Genoe, P. Heremans, J. Poortmans, Solar cells utilizing small molecular weight organic semiconductors, Prog. Photovoltaics Res. Appl. 15 (8) (2007 Dec) 659–676.
[47] S. Karadeniz, D.E. Yıldız, Frequency dependent dielectric spectroscopy of Au/n-Si structure with stannic oxide (SnO2) interfacial layer, J. Mater. Sci. Mater. Electron. 34 (18) (2023 Jun) 1416.
[48] A. Yeşildağ, M. Erdoğan, Sevgili Ö, Z. Çaldıran, İ. Orak, Optical and electrical properties of pyrene–imine organic interface layer based on p-Si, J. Electron. Mater. 50 (2021 Nov) 6448–6458.
[49] A.B. Ulusan, A.D. Tataroglu, Ş. Altındal, Y. Azizian-Kalandaragh, Photoresponse characteristics of Au/(CoFe2O4-PVP)/n-Si/Au (MPS) diode, J. Mater. Sci. Mater. Electron. 32 (12) (2021 Jun) 15732–15739.
[50] S. Khalili, H.M. Chenari, F. Yıldırım, Z. Orhan, S. Aydogan, Highly sensitive, self-powered photodetector based on reduced graphene oxide-polyvinyl pyrrolidone fibers (Fs)/p-Si heterojunction, J. Alloys Compd. 889 (2021 Dec 31), 161647.
[51] A.M. El-Mahalawy, M.A. Salam, Fabrication and photoresponse characteristics of high rectification photodetector based on methyl violet nanoparticles-PVA/p-si heterojunction for optoelectronic applications, Appl. Phys. A 126 (2020 Jun) 1–4.
[52] B. Gündüz, N. Turan, E. Kaya, N. Colak, The photo-electrical properties of the p-Si/Fe (II)–polymeric complex/Au diode, Synth. Met. 184 (2013 Nov 15) 73–82.
[53] S.A. Yerişkin, M. Balbaşı, İ. Orak, The effects of (graphene doped-PVA) interlayer on the determinative electrical parameters of the Au/n-Si (MS) structures at room temperature, J. Mater. Sci. Mater. Electron. 28 (2017 Sep) 14040–14048.
[54] O. Çiçek, H.U. Tecimer, S.O. Tan, H. Tecimer, İ. Orak, Ş. Altındal, Synthesis and characterization of pure and graphene (Gr)-doped organic/polymer nanocomposites to investigate the electrical and photoconductivity properties of Au/n-GaAs structures, Compos. B Eng. 113 (2017 Mar 15) 14–23.